Progress In Electromagnetics Research M, Vol. 46, 57–68, 2016

Microwave Scattering from Metamaterial Based Spheres in the Presence of a Conducting Plane: Normal Incidence

Adnan Jamil* **and Tenneti C. K. Rao**

Abstract—The microwave scattering characteristics of a metamaterial (MTM) sphere and an MTM coated conducting sphere is compared to that of its DPS (Real(ε) > 0, Real(μ) > 0) counterpart in the presence of an infinite conducting plane using the multipole expansion method and is presented in this article. The DPS medium may be an artificial dielectric or natural dielectric. The differential scattering cross sections and the differential backscattering cross sections of the different types of spheres are presented for a circularly polarized (left or right) beam incident normally on the sphere. The results presented may be useful for maritime applications.

1. INTRODUCTION

In this paper the theoretical scattering characteristics of microwaves from a sphere made of MTMs and a conducting sphere coated with MTMs, in the presence of an infinite conducting plane are presented. The motivation for this research arose from the works of Johnson [1] in which similar analysis is presented but with a dielectric sphere. The multipole expansion method was made use of in that effort to present the scattering characteristics of a dielectric sphere in the presence of a conducting plane. Methods used previously (references therein Johnson [1]) were approximation methods. The multipole expansion method is not an approximation, but rather provides a numerically exact solution to Maxwell's equations. The underlying principle used in this analysis is based on image theory, which has been extensively studied and researched (references therein Johnson [1]). The results presented in this paper may be useful for maritime applications [2, 3] and were obtained from computations performed by a program written in MATLAB.

2. THEORY

In this section the problem definition and methodology is presented. A sphere made of either double negative/DNG ($\varepsilon < 0$, $\mu<0$), double positive/DPS ($\varepsilon > 0$, $\mu > 0$) or dispersive MTM and a conducting sphere coated with such materials are placed in the vicinity of an infinitely long perfectly conducting plane. An incident circularly polarized (left or right) electromagnetic wave $\mathbf{E}_{inc}$ is travelling downwards normally in the negative z-direction as shown in Fig. 1. This gives rise to a reflected plane wave $\mathbf{E}_{ref}$ and scattered wave $\mathbf{E}_{scat}$. Thus the total field outside the scattering particle is the sum of all the three fields, which satisfy Maxwell's equations. A time-dependence of the form $e^{-j\omega t}$, where ω is the angular frequency of the incident wave, is assumed and suppressed throughout. All boundary conditions on the sphere surface and on the infinite conducting plane (at $z = 0$) must be satisfied.

The solution to this scattering problem is quite difficult to obtain and thus to simplify it a technique similar to *method of images* is introduced [1]. For the analysis of the system in Fig. 1, the method of

Received 22 November 2015, Accepted 10 January 2016, Scheduled 21 January 2016
* Corresponding author: Adnan Jamil (metamaterial.jamil@gmail.com).
The authors are with the Department of Electrical and Computer Engineering, University of Massachusetts Lowell, Lowell, Massachusetts, USA.

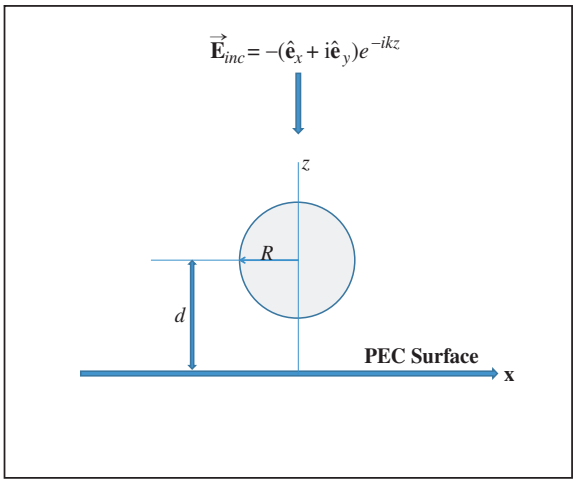

Figure 1. Physical system and geometry of the problem.

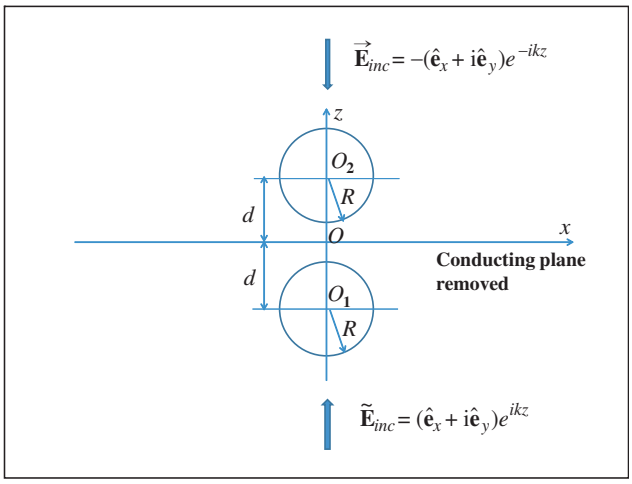

Figure 2. Geometry of the transformed system of Fig. 1 using the method of images.

images combined with the multipole expansion is employed to find the solution. By the method of images, the system in Fig. 1 will look like the transformed system in Fig. 2.

The incident field on the transformed system as shown in Fig. 2, is given by $\mathbf{E}_{inc} = -(\hat{\mathbf{e}}_x + \mathbf{i}\hat{\mathbf{e}}_y)e^{-ikz}$. An image incident field, $\tilde{\mathbf{E}}_{inc} = (\hat{\mathbf{e}}_x + \mathbf{i}\hat{\mathbf{e}}_y)e^{ikz}$ is also present. k is the wavevector in free space. The total incident wave for the two particle problem is the sum of these two waves:

$$\mathbf{E}_i = (\hat{\mathbf{e}}_x + \mathbf{i}\hat{\mathbf{e}}_y)(e^{ikz} - e^{-ikz}) \tag{1}$$

The total electric field of the system may be written as the sum of the incident wave and the scattered waves from the two particle system. In the region above the conducting plane ($z > 0$), the total electric field is the sum of the incident field and the fields scattered by the two particles.

$$\mathbf{E} = \mathbf{E}_i + \mathbf{E}_s^{(1)} + \mathbf{E}_s^{(2)} \tag{2}$$

The two scatter electric fields, $\mathbf{E}_s^{(1)}$ and $\mathbf{E}_s^{(2)}$, propagate radially outward from the centers of the two spheres, O_1 and O_2 respectively (Fig. 2). The electric fields can be expanded in terms of vector spherical wave functions as shown below.

$$\mathbf{M}_{n,m}^{(j)} = z_n^{(j)}(kr)\, e^{im\phi}\mathbf{X}_{n,m}(\theta) \tag{3}$$

$$\mathbf{N}_{n,m}^{(j)} = \frac{e^{im\phi}}{kr}\left\{\frac{\partial}{\partial r}\left[r z_n^{(j)}(kr)\right]\mathbf{Y}_{n,m}(\theta) + z_n^{(j)}(kr)\,\mathbf{Z}_{n,m}(\theta)\right\} \tag{4}$$

where, $z_n^{(j)}$ is a spherical Bessel function of type j_n, $h_n^{(1)}$ for $j = 1, 3$ respectively. The vector functions $\mathbf{X}$, $\mathbf{Y}$ and $\mathbf{Z}$ are defined by:

$$\mathbf{X}_{n,m}(\theta) = i\pi_{n,m}(\theta)\,\hat{\mathbf{e}}_\theta - \tau_{n,m}(\theta)\hat{\mathbf{e}}_\phi \tag{5}$$

$$\mathbf{Y}_{n,m}(\theta) = \tau_{n,m}(\theta)\,\hat{\mathbf{e}}_\theta + i\pi_{n,m}(\theta)\,\hat{\mathbf{e}}_\phi \tag{6}$$

$$\mathbf{Z}_{n,m}(\theta) = n(n+1)P_n^m(\cos(\theta))\,\hat{\mathbf{e}}_r \tag{7}$$

where,

$$\pi_{n,m}(\theta) = \frac{m}{\sin(\theta)}P_n^m(\cos(\theta)) \tag{8}$$

$$\tau_{n,m}(\theta) = \frac{\partial}{\partial\theta}P_n^m(\cos(\theta)) \tag{9}$$

The function $P_n^m(x)$ is the associated Legendre polynomial and ($\hat{\mathbf{e}}_r$, $\hat{\mathbf{e}}_\theta$, $\hat{\mathbf{e}}_\phi$) are unit orthogonal vectors associated with the spherical coordinates r, θ, ϕ. In the analysis that follows $\mathbf{M}_{n,m}$ and $\mathbf{N}_{n,m}$ with

$m = 1$ will be needed only. Thus $\mathbf{M}_{n,m}$ and $\mathbf{N}_{n,m}$ will be replaced with $\mathbf{M}_n$ and $\mathbf{N}_n$, respectively. The circularly polarized plane wave can be expanded and written as:

$$(\hat{\mathbf{e}}_x + \mathbf{i}\hat{\mathbf{e}}_y)\, e^{\pm ikz} = \mp \sum\nolimits_{n=1}^{\infty} (\pm i)^{n+1} \frac{2n+1}{n\,(n+1)} \left[\mathbf{M}_n^{(1)}(r,\theta,\phi) \pm \mathbf{N}_n^{(1)}(r,\theta,\phi)\right] \tag{10}$$

r, θ, ϕ are coordinates with respect to the coordinate axes with origin, O, as shown in Fig. 2. A point in this coordinate space will be represented by r. The other two coordinate systems with origins O_1 and O_2 will have points represented by r_j with coordinates (r_j, θ_j, ϕ_j), where the subscript j may be 1 or 2 depending on which origin is being referred to. The incident wave, given by Eq. (1) can be expanded in terms of spherical wave functions centered at O_1:

$$\mathbf{E}_i\,(\mathbf{r}_1) = \sum\nolimits_{n=1}^{\infty} \left[p_n \mathbf{M}_n^{(1)}\,(\mathbf{r}_1) + q_n \mathbf{N}_n^{(1)}\,(\mathbf{r}_1)\right] \tag{11}$$

The expansion coefficients in this equation can be obtained using Eq. (10). They are given by:

$$p_n = -i^{n+1} \frac{2n+1}{n\,(n+1)} \left[e^{-ikd} - (-1)^n\, e^{ikd}\right] \tag{12}$$

$$q_n = -i^{n+1} \frac{2n+1}{n\,(n+1)} \left[e^{-ikd} + (-1)^n\, e^{ikd}\right] \tag{13}$$

where d is the displacement of the center of the sphere from origin O. Also the scattered waves $E_s^{(1)}$ and $E_s^{(2)}$ can be expanded around centers O_1 and O_2, respectively.

$$\mathbf{E}_s^{(j)}\,(\mathbf{r}_j) = \sum\nolimits_{n=1}^{\infty} \left[a_n^{(j)} \mathbf{M}_n^{(3)}\,(\mathbf{r}_j) + b_n^{(j)} \mathbf{N}_n^{(3)}\,(\mathbf{r}_j)\right]; \quad j = 1, 2 \tag{14}$$

The scattering coefficients $a_n^{(1)}$, $b_n^{(1)}$, $a_n^{(2)}$ and $b_n^{(2)}$ are to be determined by the calculation. This can be made easier by taking advantage of the mirror symmetry of the system and the boundary conditions on the $z = 0$ plane. These conditions imply the following relations between the scattering coefficients:

$$a_n^{(1)} = -\,(-1)^n\, a_n^{(2)} \tag{15}$$

$$b_n^{(1)} = (-1)^n\, b_n^{(2)} \tag{16}$$

To find the scattering coefficients, it is convenient to expand the fields in the coordinate system with the origin at O_1. The fields $\mathbf{E}_i$ and $\mathbf{E}_s^{(1)}$ are already in this form. $\mathbf{E}_s^{(2)}$ is not, but can be converted to this form by means of the translation-addition theorem for vector spherical wave functions [1]. From this theorem we obtain the following:

$$\mathbf{M}_n^{(3)}\,(\mathbf{r}_2) = \sum\nolimits_{n'=1}^{\infty} \left[A_{n,n'} \mathbf{M}_{n'}^{(1)}\,(\mathbf{r}_1) + B_{n,n'} \mathbf{N}_{n'}^{(1)}\,(\mathbf{r}_1)\right] \tag{17}$$

$$\mathbf{N}_n^{(3)}\,(\mathbf{r}_2) = \sum\nolimits_{n'=1}^{\infty} \left[A_{n,n'} \mathbf{N}_{n'}^{(1)}\,(\mathbf{r}_1) + B_{n,n'} \mathbf{M}_{n'}^{(1)}\,(\mathbf{r}_1)\right] \tag{18}$$

The formulas for the coefficients $A_{n,n'}$ and $B_{n,n'}$ and a discussion of the method for calculating these are given in Appendix A. The electric field in the region outside the sphere is given by Eq. (2). The multipole expansion of this field around origin O_1 can be derived with Eqs. (11), (14), (17) and (18). The result is:

$$\begin{aligned} \mathbf{E} = \sum\nolimits_n \Bigg\{ & \left[p_n + \sum\nolimits_{n'} \left(A_{n',n} a_{n'}^{(2)} + B_{n',n} b_{n'}^{(2)}\right)\right] \mathbf{M}_n^{(1)}\,(\mathbf{r}_1) + a_n^{(1)} \mathbf{M}_n^{(3)}\,(\mathbf{r}_1) \\ & + \left[q_n + \sum\nolimits_{n'} \left(B_{n',n} a_{n'}^{(2)} + A_{n',n} b_{n'}^{(2)}\right)\right] \mathbf{N}_n^{(1)}\,(\mathbf{r}_1) + b_n^{(1)} \mathbf{N}_n^{(3)}\,(\mathbf{r}_1) \Bigg\} \end{aligned} \tag{19}$$

This equation is of the form:

$$\mathbf{E} = \sum\nolimits_n \left(\alpha_n \mathbf{M}_n^{(1)}\,(\mathbf{r}_1) + a_n^{(1)} \mathbf{M}_n^{(3)}\,(\mathbf{r}_1) + \beta_n \mathbf{N}_n^{(1)}\,(\mathbf{r}_1) + b_n^{(1)} \mathbf{N}_n^{(3)}\,(\mathbf{r}_1)\right) \tag{20}$$

The ratio of the amplitudes of scattered wave multipoles ($\mathbf{M}^{(3)}$ and $\mathbf{N}^{(3)}$) to the incident wave multipoles ($\mathbf{M}^{(1)}$ and $\mathbf{N}^{(1)}$) are:

$$u_n = \frac{a_n^{(1)}}{\alpha_n} \tag{21}$$

$$v_n = \frac{b_n^{(1)}}{\beta_n} \tag{22}$$

The quantities u_n and v_n are elements of the scattering T matrix for the particle [1]. For a homogenous sphere u_n and v_n are the Mie theory coefficients for the TE and TM scattering modes, respectively. The formulas for u_n and v_n are given in Appendix B. After u_n and v_n have been computed, these equations can be cast in a much more compact form by expressing all the coefficients as square matrices or column vectors. The quantities $a_n^{(1)}$, $b_n^{(1)}$, $a_n^{(2)}$, $b_n^{(2)}$, p_n and q_n are elements of column vectors of length N: $\mathbf{a}^{(1)}$, $\mathbf{b}^{(1)}$, $\mathbf{a}^{(2)}$, $\mathbf{b}^{(2)}$, $\mathbf{p}$ and $\mathbf{q}$. The quantities $A_{n',n}$ and $B_{n',n}$ are elements of the N by N square matrices $\mathbf{A}$ and $\mathbf{B}$. The scattering coefficients u_n and v_n are elements of the diagonal matrices $\mathbf{u} = [u_n\delta_{n,n'}]$ and $\mathbf{v} = [v_n\delta_{n,n'}]$. Also another diagonal matrix $\mathbf{g}$ is present given by $\mathbf{g} = [(-1)^n\delta_{n,n'}]$. The set of $2N$ linear equations can now be written in a matrix form:

$$\begin{bmatrix} \mathbf{A}^T + \mathbf{g}\mathbf{u}^{-1} & \mathbf{B}^T \\ \mathbf{B}^T & \mathbf{A}^T - \mathbf{g}\mathbf{v}^{-1} \end{bmatrix} \begin{bmatrix} \mathbf{a}^{(2)} \\ \mathbf{b}^{(2)} \end{bmatrix} = - \begin{bmatrix} \mathbf{p} \\ \mathbf{q} \end{bmatrix} \tag{23}$$

where Eqs. (15) and (16) gives $\mathbf{a}^{(1)} = -\mathbf{g}\mathbf{a}^{(2)}$ and $\mathbf{b}^{(1)} = \mathbf{g}\mathbf{b}^{(2)}$. The superscript T represents transpose of the matrix. Scripts written in MATLAB were used to solve this matrix equation and calculate the scattering coefficients. Once the scattering coefficients $\mathbf{a}^{(2)}$ and $\mathbf{b}^{(2)}$ have been calculated the next step is to find the differential cross sections and differential backscattering cross sections.

The scattered wave is the sum of the two scattering components:

$$\mathbf{E}_{scat} = \mathbf{E}_s^{(1)} + \mathbf{E}_s^{(2)} \tag{24}$$

The asymptotic form of this wave can be evaluated in the limit $r \to \infty$ with the aid of Eq. (14) to obtain:

$$\mathbf{E}_{scat} = \frac{e^{ikr}}{ikr} e^{i\phi} [S_\theta(\theta)\,\hat{\mathbf{e}}_\theta + iS_\phi(\theta)\,\hat{\mathbf{e}}_\phi] \tag{25}$$

where, the vector components of the scattering amplitude are given by:

$$S_\theta(\theta) = e^{ikdcos(\theta)} S_\theta^{(1)}(\theta) + e^{-ikdcos(\theta)} S_\theta^{(2)}(\theta) \tag{26}$$

$$S_\phi(\theta) = e^{ikdcos(\theta)} S_\phi^{(1)}(\theta) + e^{-ikdcos(\theta)} S_\phi^{(2)}(\theta) \tag{27}$$

and where:

$$S_\theta^{(j)}(\theta) = -\sum\nolimits_{n=1}^{N} (-i)^{n+1} \left[a_n^{(j)} \pi_n(\theta) + b_n^{(j)} \tau_n(\theta) \right] \tag{28}$$

$$S_\phi^{(j)}(\theta) = -\sum\nolimits_{n=1}^{N} (-i)^{n+1} \left[a_n^{(j)} \tau_n(\theta) + b_n^{(j)} \pi_n(\theta) \right] \tag{29}$$

for $j = 1, 2$.

If the incident beam is right or left circularly polarized or if it is unpolarized, as considered in the paper, the differential scattering cross section (DSCS) is given by [1]:

$$\sigma(\theta) = \frac{1}{2k^2} \left[|S_\theta(\theta)|^2 + |S_\phi(\theta)|^2 \right] \tag{30}$$

The angle θ in these formulas is restricted to the reflecting plane, i.e., $0 \le \theta \le \frac{\pi}{2}$. For the differential backscattering cross section (DBSCS), θ is set to 0° and a frequency sweep is performed. In all cases, $10 * \log_{10}(\frac{\sigma}{\pi R^2})$ is the quantity sought and plotted, with R being the radius of the object i.e., sphere or coated sphere. The next section will present some results and discussion on the DSCS and DBSCS of MTM based spheres in the presence of a conducting plane.

3. RESULTS

In this section, some representative results of the scattering characteristics of MTM spheres and MTM coated conducting spheres in the presence of a perfectly conducting plane are presented and compared to its dielectric DPS counterpart. The analysis that follows is in the microwave regime (0.1 GHz–10 GHz) and the findings should be of benefit to the maritime engineering community [2, 3]. The types of material considered are dielectrics (artificial or natural) and DNG type MTM of both lossless and lossy kinds. In the first part the results of scattering from an MTM and dielectric sphere will be discussed and in the second part a conducting sphere coated by a layer of MTM and dielectric will be looked at.

3.1. Scattering from a Dielectric/MTM Sphere

The scattering characteristics of a normally incident circularly polarized (left or right) wave from a dielectric and MTM sphere will be studied and compared in this section. A sphere of radius 50 mm is considered in the configuration of Fig. 1. For the nondispersive MTM sphere only DNG type was considered. In the dispersive case the MTM layer may act as DNG, DPS, ENG or MNG depending on the frequency spectrum considered. Both the DBSCS and DSCS results were obtained and comparisons were made between materials of different electromagnetic properties. Below are some representative results and discussions.

Figure 3 shows the DBSCS characteristics for a DPS sphere ($\varepsilon_r = 2.54$ and $\mu_r = 2$) and a DNG sphere ($\varepsilon_r = -2.54$ and $\mu_r = -2$). The conducting plane is at a distance of 0.275 m from the center of the sphere. The distance is chosen such that it is comparable to the radius of the sphere. From the figure it can be observed that for low frequencies, lower than approximately 1 GHz, the backscattering from the DNG sphere is much higher than that of the DPS sphere, indicating that at lower frequencies and with these material parameters, the DNG sphere is a highly scattering structure in this configuration. At frequencies between 1.4 GHz to 2.6 GHz, the backscattering from the DNG sphere is at lower levels than that of the DPS sphere. Beyond 4 GHz, there is not much difference between backscattering of the two. Next, further investigation is done to study the DSCS of the two spheres under different conditions.

Figure 4 shows the DSCS characteristic of DPS spheres with different ε_r values and a fixed value for μ_r at 2 at an incident frequency of 2.5 GHz. For $\varepsilon_r = 2.54$ in the backscattering direction ($\theta = 0°$), the scattering level is roughly at 10.5 dB which matches the backscattering level at $f = 2.5$ GHz in Fig. 3. Of the three different ε_r values the lowest overall scattering in all directions is the lowest for $\varepsilon_r = 0.001$, which approximates nihility media with very low refractive index. Fig. 5 shows results for the same exact scenario except the sphere is a DNG sphere. For $\varepsilon_r = -2.54$ in the backscattering direction ($\theta = 0°$), the scattering level is roughly at 0 dB which matches the backscattering level in Fig. 3. The lowest overall scattering in all directions is observed for $\varepsilon_r = -2.54$, unlike that of the DPS case. The scattering from the nihility approximated media ($\varepsilon_r = -0.001$) is the most scattering until approximately $\theta = 67°$, indicating that the scattering levels are, overall, the lowest for planes close to the azimuthal plane ($\theta = 90°$) in the nihility media case. By keeping ε_r fixed, the effect of variation of μ_r is studied next.

Figure 6 is representative of the DSCS characteristics for a DPS sphere for different values of μ_r with ε_r fixed at 2.54. For $\mu_r = 2$ in the backscattering direction ($\theta = 0°$), the scattering level is roughly at 10.5 dB which matches the backscattering level at $f = 2.5$ GHz in Fig. 3. Apart from the main lobe ($0° \leq \theta \leq\sim 27°$), a non-monotonically varying set of scattering characteristics is observed in all directions with increasing μ_r. For planes closer to the azimuthal plane ($\theta \geq 60°$) the scattering is lower than 0 dB for $\mu_r = 1$ and $\mu_r = 3$. In Fig. 7, for the $\mu_r = -2$ in the backscattering direction

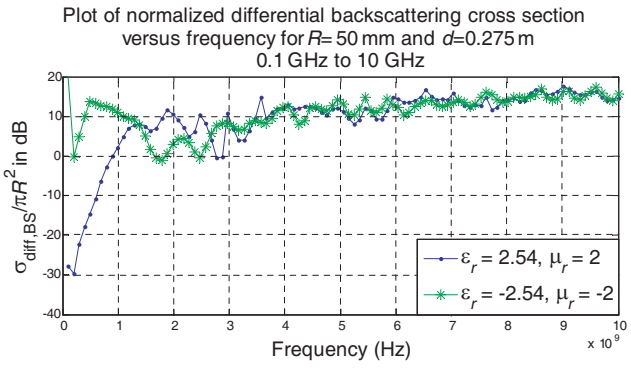

Figure 3. Differential backscattering cross section characteristics for non-dispersive DPS and DNG MTM sphere in the presence of a conducting plane.

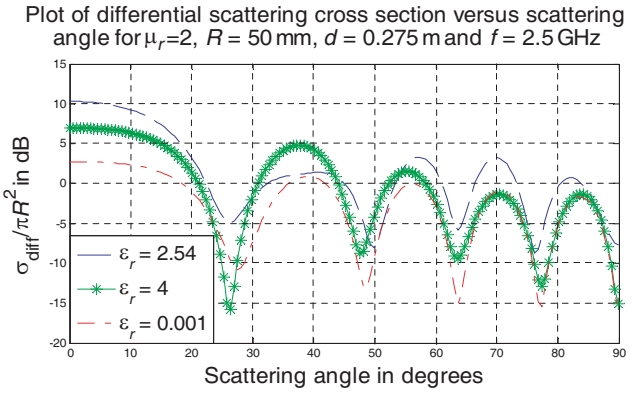

Figure 4. DSCS characteristics of DPS spheres with different ε_r values.

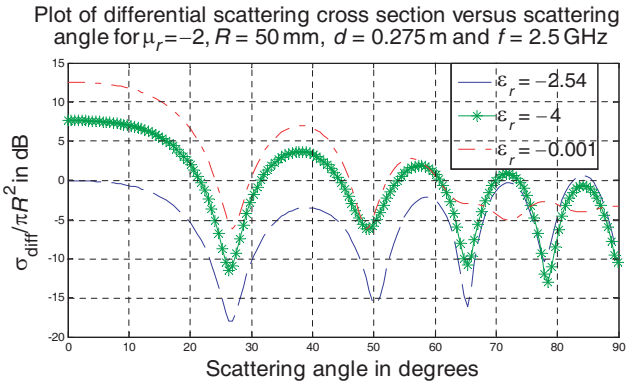

Figure 5. DSCS characteristics of DNG spheres with different ε_r values.

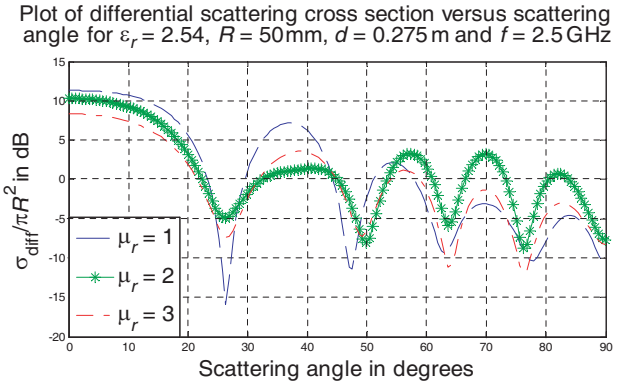

Figure 6. DSCS characteristics of DPS spheres with different μ_r values.

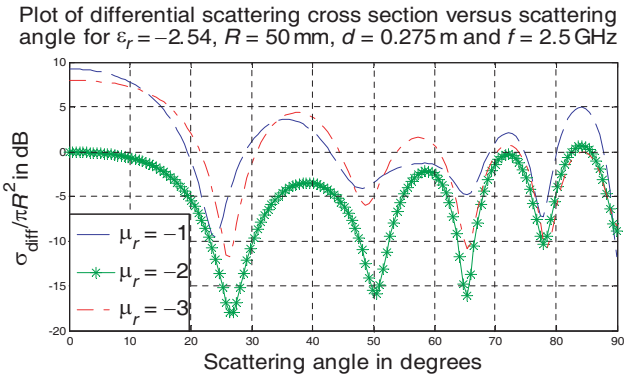

Figure 7. DSCS characteristics of DNG spheres with different μ_r values.

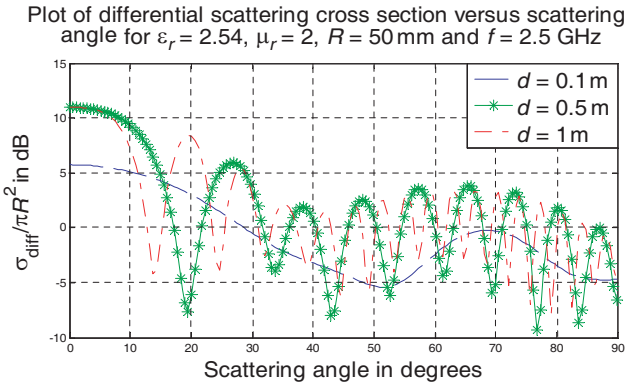

Figure 8. DSCS characteristics for a DPS sphere at different heights of placement from the conducting plane.

($\theta = 0°$), the scattering level is roughly at 0 dB which matches the backscattering level at $f = 2.5$ GHz in Fig. 3. A similar non-monotonically varying set of patterns is observed with the DNG case of Fig. 7 when scattering levels are compared to each other for all three cases apart from the lobe close to the azimuthal plane ($80° \leq \theta \leq 90°$), where the scattering levels are monotonically decreasing with decreasing value of μ_r. An interesting feature is that for the $\mu_r = -2$ case the scattering is below 0 dB for almost all directions, except it creeps just above 0 dB for a small range of scattering angles above 80°. The scattering characteristics for fixed values of ε_r and μ_r for different heights of placement of the sphere are looked at next.

Figure 8 shows the DSCS characteristics for a DPS sphere at different heights of placement ($d = 0.1$ m, 0.5 m and 1 m) at a frequency of 2.5 GHz. It can be observed that as height increases, the characteristics starts to increase in the number of lobes. The backscattering ($\theta = 0°$) is the lowest for the smallest height ($d = 0.1$ m) for the DPS sphere at roughly 6 dB. As height increases, there is not much change in the backscattering levels as can be observed with $d = 0.5$ m and 1 m. A similar characteristic is observed with the DNG sphere of Fig. 9, with the number of lobes increasing as the height increases, but there is not much change in the backscattering levels and remains almost at a constant level of roughly 0 dB. The overall patterns for all three heights remain on or below 0 dB for all scattering directions. The analysis for non-dispersive DPS and DNG spheres end with the case where the radius of the sphere is varied at fixed height and frequency.

Figure 10 shows the DSCS characteristics for a DPS sphere with varying radii at a frequency of 2.5 GHz. In the backscattering direction ($\theta = 0°$), the backscattering levels for all three are roughly between 8 dB to 12 dB. In certain ranges of scattering angles, scattering is either monotonically increasing

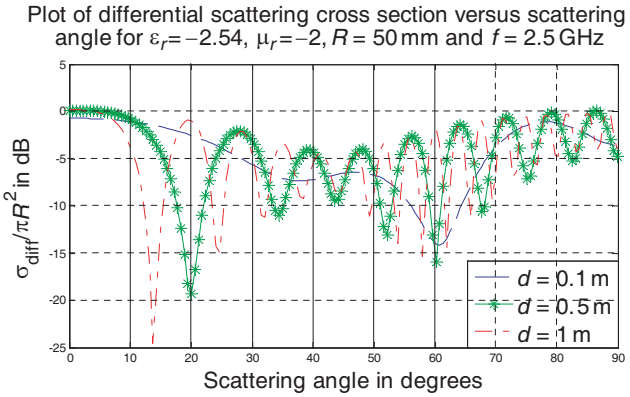

Figure 9. DSCS characteristics for a DNG sphere at different heights of placement from the conducting plane.

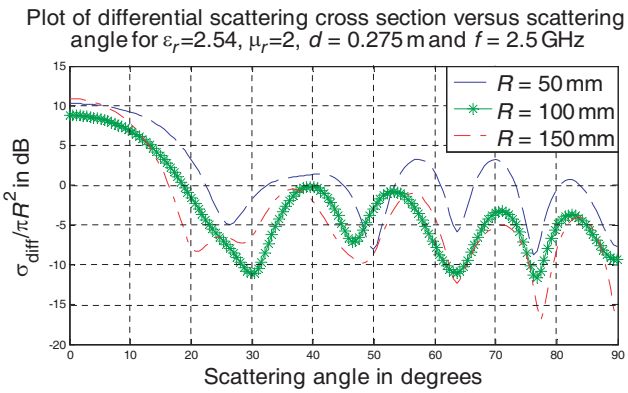

Figure 10. DSCS characteristics for a DPS sphere with different radii.

or decreasing with increasing radius. For both $R = 100$ mm and $R = 150$ mm the scattering levels are below 0 dB for $\theta \geq 20°$. A similar behavior is observed with the DNG sphere of Fig. 11, as radius is varied. The backscattering level for $R = 50$ mm is at 0 dB with the overall pattern hovering at or below 0 dB in all directions. This is in contrast to $R = 100$ mm and $R = 150$ mm, where the backscattering is above 10 dB. All these results encourage the investigation scattering from dispersive DPS and DNG sphere in the presence of a conducting plane.

For the dispersion model, the Drude-Lorentz model for the rings and rods type of MTM was investigated [4–6]. The MTM relative permittivity, ε_r, and relative permeability, μ_r, as a function of frequency is given by:

$$\varepsilon_r = 1 - \frac{f_p^2}{f^2 + jf\gamma_e} \tag{31}$$

$$\mu_r = 1 - \frac{f_{mp}^2 - f_o^2}{f - f_o^2 + jf\gamma_h} \tag{32}$$

where, electric and magnetic collision frequencies are γ_e and γ_h, respectively; magnetic resonance frequency is f_o; plasma frequency is f_p; f_{mp} is the magnetic plasma frequency. An examination of any dispersive MTM show that for certain frequency bands, the MTM may act as DPS ($\mathrm{Re}(\varepsilon_r) > 0$, $\mathrm{Re}(\mu_r) > 0$), DNG ($\mathrm{Re}(\varepsilon_r) < 0$, $\mathrm{Re}(\mu_r) < 0$), ENG ($\mathrm{Re}(\varepsilon_r) < 0$, $\mathrm{Re}(\mu_r) > 0$) or MNG ($\mathrm{Re}(\varepsilon_r) > 0$, $\mathrm{Re}(\mu_r) < 0$). For the time dependence chosen in this paper and to maintain consistency with Poynting's theorem, the imaginary parts of the two parameters need to be positive. The characteristic parameters of the coating layer are therefore given by:

$$\varepsilon_r = \pm\varepsilon' + j\varepsilon'' \tag{33}$$

$$\mu_r = \pm\mu' + j\mu'' \tag{34}$$

$$k_{sph} = \pm k' + jk'' \tag{35}$$

$$\eta_{sph} = \eta' \pm j\eta'' \tag{36}$$

k_{sph} is the wavevector within the MTM sphere or coating. It should be noted that the lossless DNG case $k_{sph} = -k'$ and for the lossless ENG case $\eta_{sph} = -j\eta''$ [6]. To model the dielectric DPS nature, the real parts of ε_r and μ_r are forced to be positive for the entire frequency range. The material properties and DBSCS characteristics of a dispersive and lossy DPS dielectric and DNG MTM sphere in the presence of a conducting plane are shown next.

Figure 12 shows the permittivity and permeability properties of a dispersive rings and rods media based on the Drude/Lorentz model of Eqs. (31) and (32). It approximates a DNG material between approximately 2.5 GHz to 4 GHz, i.e., both ε_r and μ_r have negative real parts within that frequency band. On the other hand, Fig. 13 shows a hypothetical DPS dielectric material which is modeled by

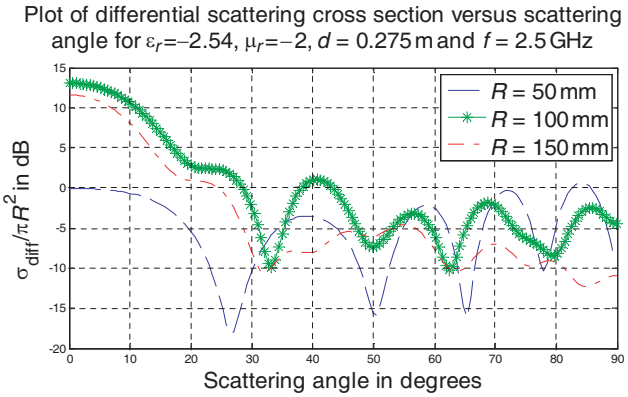

Figure 11. DSCS characteristics for a DNG sphere with different radii.

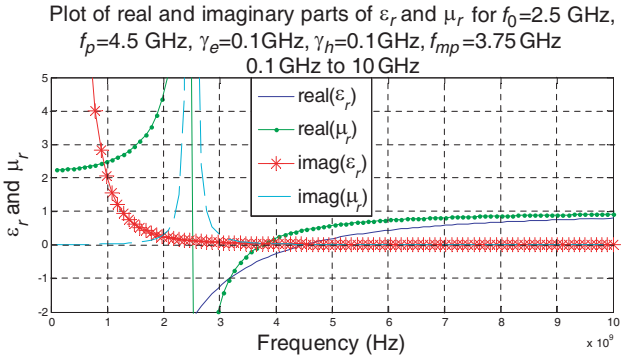

Figure 12. Characteristics of a dispersive DNG MTM.

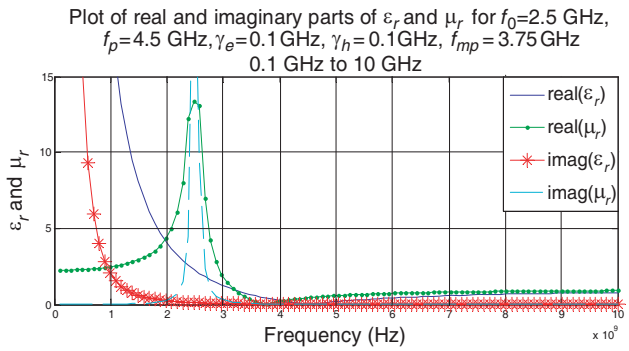

Figure 13. Characteristics of a dispersive hypothetical dielectric DPS material.

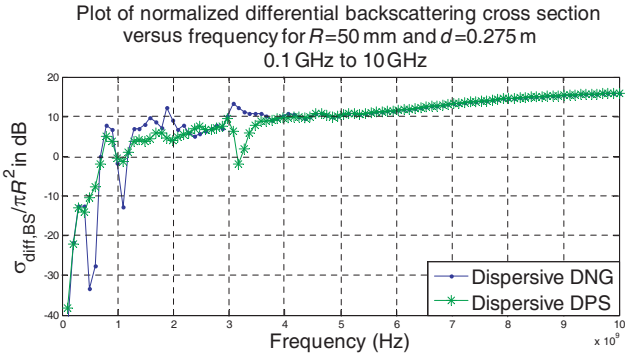

Figure 14. Comparison of DBSCS characteristics of a dispersive DPS and dispersive DNG sphere.

the same exact characteristics of the Drude/Lorentz model used for the DNG media of Fig. 12, except that the absolute value of the real parts of both ε_r and μ_r are considered for the entire frequency range, thus rendering it a DPS dielectric material. The scattering characteristics of a sphere made of both these materials in the presence of a conducting plane will be studied and compared.

Figure 14 shows a comparison of the DBSCS characteristics of a DPS and DNG sphere for a height of 0.275 m. It may observed that at the lower end of the frequency range, between 0.1 GHz to 2 GHz, there are regions where the DNG sphere has a much weaker scattering than its DPS counterpart. For the DNG sphere there are narrow bands centered around 0.5 GHz and 1.15 GHz where the backscattering levels are below −10 dB. Also in the region between 1.25 GHz to 2.25 GHz, the DNG sphere has a stronger backscattering than it DPS counterpart. In the frequency band of 3 GHz to 3.75 GHz the DNG sphere has a stronger backscattering as well. Fig. 15 shows the effect of height on backscattering levels below −10 dB for the DNG sphere. For a reduced height of 0.25 m the frequency band centered around 1.15, for which backscattering levels are below −10 dB, disappears. When a conducting sphere is coated with these materials interesting effects are expected for scattering enhancement and reduction which may be beneficial for both detection and cloaking for maritime applications.

3.2. Scattering from a Dielectric/MTM Coated Conducting Sphere

In this section, a conducting sphere of 50 mm radius will be coated by a layer of dielectric and DNG MTM and comparisons of the DBSCS will be made between the two. Furthermore it can be shown that adding a layer of MTM will reduce the DBSCS significantly and this will be beneficial for cloaking a conducting object in the presence of a conducting plane. Also scattering may be enhanced and this will

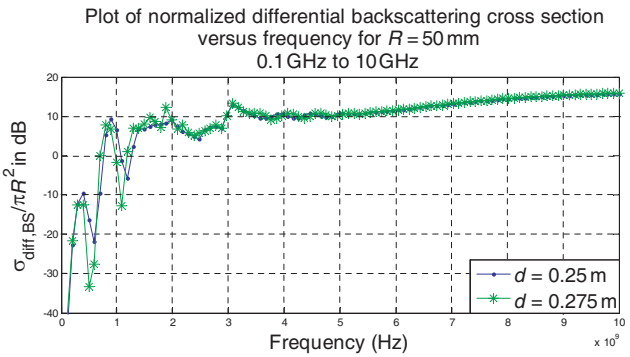

Figure 15. Comparison of DBSCS characteristics of a dispersive DNG sphere at different heights.

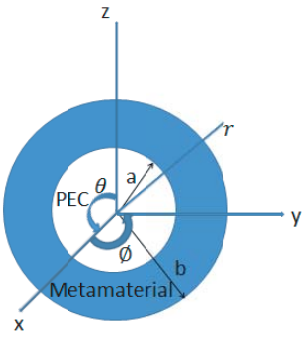

Figure 16. Geometry of the coated sphere.

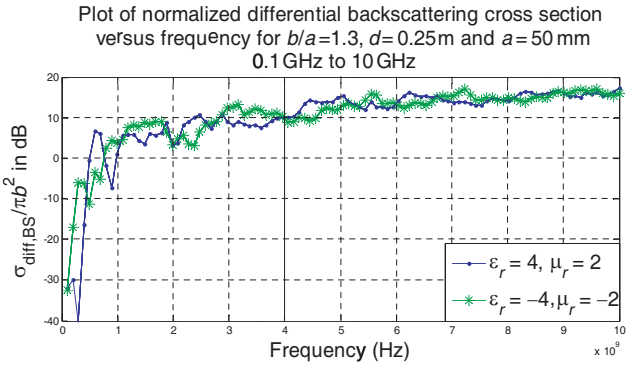

Figure 17. Comparison of DBSCS characteristics between lossless DPS dielectric coated and lossless DNG MTM coated conducting sphere.

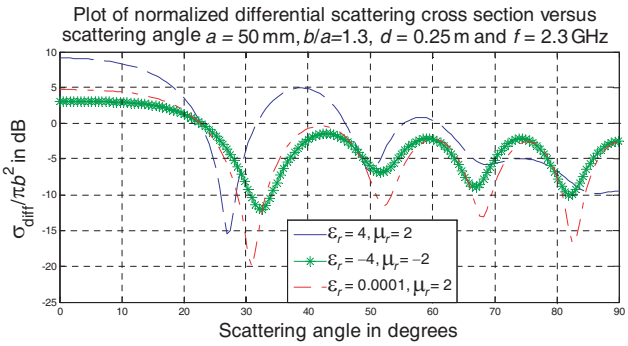

Figure 18. DSCS of a conducting sphere coated with different lossless materials.

be useful for detection purposes. The scattering coefficients u_n and v_n will change for the coated sphere as given in Appendix B. The geometry of the coated sphere is shown below in Fig. 16. The dielectric or MTM layer may be lossless or lossy. The aspect ratio, b/a, is a measure of the thickness of the MTM layer.

Figure 17 shows the DBSCS characteristics of a conducting sphere coated with a lossless dielectric and lossless DNG MTM for an aspect ratio of 1.3 and at a height of 0.25 m. The characteristics show that there are different frequency spectra where one kind of coating may scatter more or less than the other, and thus shows that lossless DNG media may not be advantageous for cloaking applications for the overall frequency range. If one were to focus on a specific frequency band then only can lossless DNG media be useful for scattering reduction applications. An example of this is in the spectrum between roughly 2 GHz to 2.6 GHz where the DNG coating causes less scattering then its dielectric counterpart. If a frequency of 2.3 GHz was chosen and a plot of the DSCS was made, as shown in Fig. 18, then it may be observed that overall scattering is much lower for the DNG case then the dielectric/DPS case which can be helpful for cloaking applications. These results encourage the study of introducing dispersion into the coating material and observe its effects.

Figure 19 shows the DBSCS characteristics for a dispersive DNG and dispersive DPS coated sphere for an aspect ratio of 1.3 and at a height of 0.275 m from the conducting plane. The relative permeability and relative permittivity characteristics of the dispersive DNG and DPS are that of Figs. 12 and 13 respectively. From Fig. 19 it can be observed that there is a very narrow band in the DNG case centered around 0.8 GHz where the scattering goes down below −10 dB. There is no such band for the DPS case.

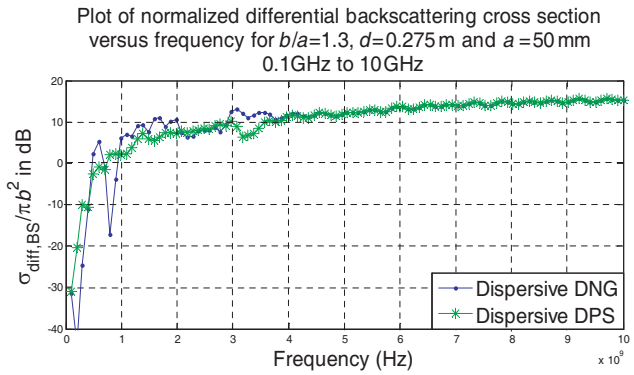

Figure 19. DBSCS of a conducting sphere coated with different lossy and dispersive materials.

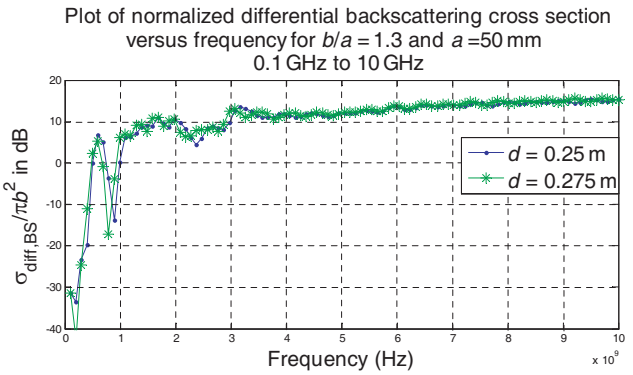

Figure 20. DBSCS of a conducting sphere coated with dispersive DNG MTM at two different heights of placement.

On the other hand, roughly between 3 GHz to 3.7 GHz DNG coating has a stronger scattering than the DPS coating. So it may be concluded that DNG type coating may be beneficial for both cloaking and detection applications. A further analysis for the DNG case is shown in the figure below (Fig. 20) where the DBSCS characteristics are shown at two different heights and the effects on the bandwidth for which backscattering is below -10 dB are shown. Several iterations of the simulation program was run by changing the height and the resonance region centred around 0.8 GHz disappeared if the sphere was placed too close or too far away from the conducting plane (not shown in the paper), indicating that height has a role in achieving optimum bandwidth for which cloaking or detectability may be achieved.

4. CONCLUSIONS

In this paper, the scattering from an MTM sphere and an MTM coated conducting sphere in the presence of a conducting plane using the multipole expansion method were presented and compared to its dielectric counterpart. The results show that utilization of MTM will potentially allow altering the scattering characteristics for maritime purposes, where sea water may be considered as a good conductor in these frequencies. Enhancement of backscattering with the MTM coating was observed for some spectrum of frequencies indicating that MTM may be useful for detection purposes. Furthermore, lowering observability of conducting spheres by coating it with a layer of MTM in the presence of conducting plane was also a feature noticed thus providing encouragement for cloaking applications. Further investigations are needed to achieve cloaking of a conducting sphere for broader spectra at higher frequencies in the presence of the conducting plane.

APPENDIX A. THE TRANSLATION-ADDITION THEOREM

The expansion coefficients $A_{n,n'}$ and $B_{n,n'}$ of Eq. (17) are given by [1]:

$$A_{n,n'} = -i^{n'-n}\frac{2n'+1}{2n'(n'+1)}\sum\nolimits_{\upsilon} i^{-\upsilon}\left[n\left(n+1\right)+n'\left(n'+1\right)-\upsilon\left(\upsilon+1\right)\right]\cdot a\left(n,n';\upsilon\right)\cdot h_{\upsilon}^{(1)}(k\delta) \quad \text{(A1)}$$

$$B_{n,n'} = i^{n'-n}\frac{2n'+1}{2n'(n'+1)}\sum\nolimits_{\upsilon} i^{-\upsilon}(2ik\delta)\cdot a\left(n,n';\upsilon\right)\cdot h_{\upsilon}^{(1)}(k\delta) \quad \text{(A2)}$$

where $h_{\upsilon}^{(1)}(k\delta)$ is the spherical Hankel function of the first kind and $a(n,n';\upsilon)$ is special form of the Guant coefficient, defined by the following product of two $3-j$ symbols:

$$a\left(n,n';\upsilon\right) = (2\upsilon+1)\left[\frac{n\left(n+1\right)}{n'(n'+1)}\right]^{1/2}\begin{pmatrix} n & n' & \upsilon \\ 0 & 0 & 0 \end{pmatrix}\begin{pmatrix} n & n' & \upsilon \\ 1 & -1 & 0 \end{pmatrix} \quad \text{(A3)}$$

It is to be noted that $A_{n,n'} = A_{n',n}$ and $B_{n,n'} = B_{n',n}$. Also $\delta = 2d$.

APPENDIX B. FORMULAS FOR THE SCATTERING COEFFICIENTS

B.1. Scattering Coefficients for the Plain Sphere

If a sphere is made of material with relative permeability, μ_r, and relative permittivity, ε_r, then its refractive index is given by $n = \sqrt{\varepsilon_r \mu_r}$. All these quantities could be complex numbers. The wavevector within the sphere, k_{sph}, is given by $k_{sph} = nk$, where k is the wavevector in free space given by $k = \frac{2\pi}{\lambda}$. λ is the wavelength of the incident radiation on the sphere. $\hat{J}_n$ and $\hat{H}_n^1$ are Ricatti-Bessel and Hankel functions. All primes denote derivative with respect to the argument of the function. It is assumed that the medium surrounding the sphere is free space. The scattering coefficients u_n and v_n of Eq. (20) are given by [5]:

$$u_n = -\frac{\sqrt{\mu}_r \hat{J}_n(k_{sph}R)\,\hat{J}_n'(kR) - \sqrt{\varepsilon}_r \hat{J}_n(kR)\,\hat{J}_n'(k_{sph}R)}{\sqrt{\mu}_r \hat{J}_n(k_{sph}R)\,\hat{H}_n^{1\prime}(kR) - \sqrt{\varepsilon}_r \hat{H}_n^1(kR)\,\hat{J}_n'(k_{sph}R)} \tag{B1}$$

and

$$v_n = -\frac{\sqrt{\mu}_r \hat{J}_n(kR)\,\hat{J}_n'(k_{sph}R) - \sqrt{\varepsilon}_r \hat{J}_n(k_{sph}R)\,\hat{J}_n'(kR)}{\sqrt{\mu}_r \hat{H}_n^1(kR)\,\hat{J}_n'(k_{sph}R) - \sqrt{\varepsilon}_r \hat{J}_n(k_{sph}R)\,\hat{H}_n^{1\prime}(kR)} \tag{B2}$$

B.2. Scattering Coefficients for the Coated Conducting Sphere

Referring to the geometry of Fig. 16, the coating is made of material with relative permeability, μ_r, and relative permittivity, ε_r. Thus the intrinsic impedance of the coating, η_{sph}, will be $\eta_{sph} = \sqrt{\frac{\mu_r}{\varepsilon_r}} \cdot \eta_0$, where η_0 is roughly 120π and is the intrinsic impedance of free space. The wavevector within the coating, k_{sph}, is given by $k_{sph} = nk$, where k is the wavevector in free space given by $k = \frac{2\pi}{\lambda}$. n is the complex refractive index of the coating, given by $n = \sqrt{\varepsilon_r \mu_r}$ and λ is the wavelength of the incident radiation on the coated sphere. $\hat{J}_n$ and $\hat{Y}_n$ are Ricatti-Bessel functions. All primes denote derivative with respect to the argument of the function. It is assumed that the medium surrounding the coated sphere is free space. Thus the scattering coefficients u_n and v_n may now be written as [7]:

$$S_n(b) = \hat{J}_n(k_{sph}a)\,\hat{Y}_n(k_{sph}b) - \hat{J}_n(k_{sph}b)\,\hat{Y}_n(k_{sph}a) \tag{B3}$$

$$S_n'(b) = \hat{J}_n(k_{sph}a)\,\hat{Y}_n'(k_{sph}b) - \hat{J}_n'(k_{sph}b)\,\hat{Y}_n(k_{sph}a) \tag{B4}$$

$$R_n(b) = \hat{J}_n'(k_{sph}a)\,\hat{Y}_n(k_{sph}b) - \hat{J}_n(k_{sph}b)\,\hat{Y}_n'(k_{sph}a) \tag{B5}$$

$$R_n'(b) = \hat{J}_n'(k_{sph}a)\,\hat{Y}_n'(k_{sph}b) - \hat{J}_n'(k_{sph}b)\,\hat{Y}_n'(k_{sph}a) \tag{B6}$$

$$u_n = \frac{\eta_{sph}\hat{J}_n(kb)\,R_n'(b) - \eta_0 \hat{J}_n'(kb)\,R_n(b)}{\eta_0 R_n(b)\hat{H}_n^{1\prime}(kb) - \eta_{sph}\hat{H}_n^1(kb)\,R_n'(b)} \tag{B7}$$

and

$$v_n = \frac{\eta_0 \hat{J}_n(kb)\,S_n'(b) - \eta_{sph}\hat{J}_n'(kb)\,S_n(b)}{\eta_{sph} S_n(b)\hat{H}_n^{1\prime}(kb) - \eta_0 \hat{H}_n^1(kb)\,S_n'(b)} \tag{B8}$$

REFERENCES

1. Johnson, B. R., "Light scattering from a spherical particle on a conducting plane: I. Normal incidence," *J. Opt. Soc. Am. A*, Vol. 9, No. 8, 1341–1351, Aug. 1992.
2. Petrillo, L., F. Jangal, M. Darces, J.-L. Montmagnon, and M. Helier, "Surface wave enhancement using HF metamaterials," *PIERS Proceedings*, 586–588, Marrakesh, Morocco, Mar. 20–23, 2011.
3. Zhao, X.-W., C.-H. Liang, and L. Liang, "Multilevel fast multipole algorithm for radiation characteristics of shipborne antennas above seawater," *Progress In Electromagnetics Research*, Vol. 81, 291–302, 2008.
4. Ruppin, R., "Electric and magnetic energies within dispersive metamaterial spheres," *J. Opt.*, Vol. 13, No. 9, 095101-1–5, 2011.

5. Ruppin, R., "Extinction properties of a sphere with negative permittivity and permeability," *Solid State Comm.*, Vol. 116, No. 8, 411–415, 2000.
6. Oraizi, H. and A. Abdolali, "Combination of MLS, GA & CG for the Reduction of RCS of multilayered cylindrical structures composed of dispersive metamaterials," *Progress In Electromagnetics Research B*, Vol. 3, 227–253, 2008.
7. Richmond, J. H., "Scattering by a Ferrite-coated conducting sphere," *IEEE Trans. Ant. Prop.*, Vol. 35, No. 1, 73–79, Jan. 1987.